Robust Continuous Model Predictive Speed and Current Control for PMSM With Adaptive Integral Sliding-Mode Approach

Zheng Li, Fengxiang Wang, *Senior Member, IEEE*, Dongliang Ke, Jiaxiang Li, and Wei Zhang

***Abstract*—Model predictive control has been considered as a potential alternative method in electrical drives. High reliable predictive model design is a research hotspot. To further improve the performance, a robust continuous model predictive speed and current control for PMSM with an adaptive integral sliding-mode approach are put forward. The prediction model is directly derived from the integral slinging-mode surface. By using the self-regulation method control and the amplitude of the sliding-mode function, an adaptive integral sliding-mode predictive control (AISMPC) is designed. The proposed strategy solves the chattering problem of sliding-mode control and improves the dynamics of the system. AISMPC has been carried out on a digital signal processing hardware system. The experimental results validate the excellent tracking performance of the proposed strategy.**

***Index Terms*—Adaptive integral sliding-mode predictive control (AISMPC), load disturbance compensation, permanent magnet synchronous machine (PMSM).**

I. Introduction

THE progress of material science, the development of electronic chips, and the deep research of control strategy have provided an important impetus for the development of modern power electronics. Permanent magnet synchronous motor (PMSM) has been widely used in servosystems and electric vehicles due to its advantages of small size, high power density, and high reliability. Currently, the traditional proportional–integral (PI) controller is commonly used as speed and current regulating controller in field-oriented control (FOC). PI controller is also an important regulator in the speed control loop of direct torque control (DTC) and model predictive control (MPC). Although FOC and DTC methods have been widely used, the tuning of parameters and the reduction of ripples still need further research [1].

MPC is becoming an emerging control strategy in the areas of electric drives and power electronics. MPC can be classified into two categories: 1) continuous control set MPC (CCS-MPC) and 2) finite control set MPC (FCS-MPC) [2]. When controlling electrical drives, FCS-MPC contains merits such as faster dynamics, an intuitive concept of design, straightforward structure, and realization [3]. Deadbeat control (DB) is one of the CCS-MPC, whose structure has no weighting factor and less current harmonic. In the structure of MPC, the PI controller is used normally for speed loop and the model prediction controller is applied for the current loop [4].

Although the PI controller has the advantages of simple algorithm structure, high reliability, and rapid speed regulation, it is difficult to meet the precise positioning and speed regulation requirements when the external disturbance is too large or internal parameters vary greatly. To meet the higher performance requirements, many modern control theories, including active disturbance rejection control, adaptive control, optimal control, fuzzy control, and robust control, have been gradually applied to the control system of PMSM [5]–[9]. Among them, the sliding-mode controller (SMC) has been proposed to improve the closed-loop robustness against the parametric uncertainties and strong robustness to external disturbances.

Sliding-mode variable structure control is a special nonlinear control strategy, which enables the state trajectory to reach the predetermined sliding-mode surface and converge along the sliding-mode surface to state origin. Owing to the sliding mode can be designed and is independent of internal parameters and external disturbance, the variable structure control has the advantages of fast response, simple physical implementation, and strong robustness [10]–[12]. However, the exponential reaching law arriving at the sliding-mode surface speed is determined by the design value of the reaching law parameter, which makes it contradictory to increase the reaching speed and reduce the sliding chattering. To have a faster reaching performance and suppress the chattering effect at the same time, in [13] and [14], new sliding-mode reaching law is designed, which included variable speed index reaching law and achieved better

Manuscript received September 8, 2020; revised December 29, 2020 and March 23, 2021; accepted May 28, 2021. Date of publication June 4, 2021; date of current version August 16, 2021. This work was supported in part by the National Natural Science Funds of China under Grant 51877207, in part by the Science and Technology Program of Fujian Province under Grant 2020T3003, and in part by the Science and Technology Program of Quanzhou City under Grants 2020C028R, 2020C002R, and 2020C073. Recommended for publication by Associate Editor T. Dragicevic. *(Corresponding author: Fengxiang Wang.)*

Zheng Li is with the Fujian Institute of Research on the Structure of Matter, Chinese Academy of Sciences, Fuzhou 350000, China, and also with the University of Chinese Academy of Sciences, Beijing 100000, China (e-mail: lizheng4569@outlook.com).

Fengxiang Wang, Dongliang Ke, and Jiaxiang Li are with the Quanzhou Institute of Equipment Manufacturing, Haixi Institutes, Chinese Academy of Sciences, Jinjiang 362200, China (e-mail: fengxiang.wang@fjirsm.ac.cn; dongliang.ke@fjirsm.ac.cn; jiaxiang_li163@163.com).

Wei Zhang is with the Technische Universität München, 80333 Munich, Germany (e-mail: wei.zhang2@tum.de).

Color versions of one or more figures in this article are available at https://doi.org/10.1109/TPEL.2021.3086636.

Digital Object Identifier 10.1109/TPEL.2021.3086636

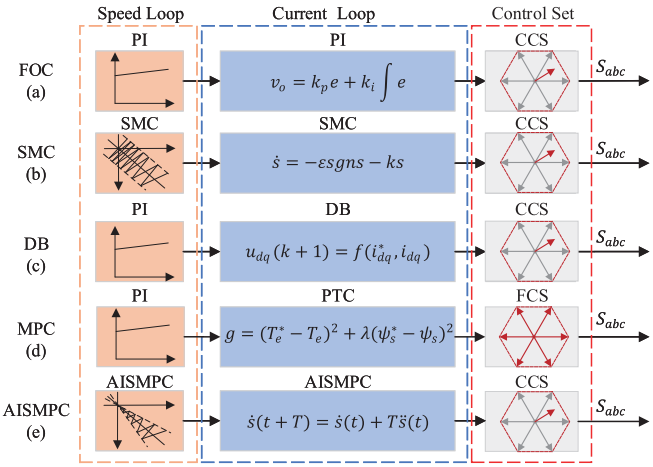

Fig. 1. Comparison of different controller structures.

performance as expected. In engineering applications, there is chattering in discrete systems. To further improve the antidisturbance ability of the system, many strategies are applied such as discrete-time SMC [15] and dynamic SMC [16]. In [17], Hassine *et al.* present an implementation of an extended model predictive-sliding-mode control reduces the execution time of the whole control algorithm significantly. A disturbance observer (DOB)-based PTC approach has been investigated in [18]–[21] for motor systems subject to load torque disturbances, parameter uncertainties, and time delays. Not only does the speed loop adopt a DOB-based feed-forward compensation method for improving the system antidisturbance ability and robustness, but also the flux, current, and torque predictions are also promoted.

This article proposes a robust continuous model predictive speed and current control for PMSM with an adaptive integral sliding-mode approach. Based on the research of SMC and MPC in deep, this article proposed a robust control strategy for PMSM. AISMPC is different from the existed predictive method, the prediction model is derived from the sliding-mode surface. Aiming at solving the chattering problem of discrete sliding-mode control approach law, an adaptive sliding-mode structure is designed. At the same time, load disturbance compensation effectively improves the antidisturbance capability of the system. As MPC is applied for both external speed and inner current controllers, fast dynamics of the system is achieved. To verify the validity, the proposed strategy is compared with FOC, SMC, DB, MPC, and other different control structures. In this article, Fig. 1 shows the comparison of various control structures, including classical control strategies and gradually improved methods. The experimental results show that the proposed strategy has the advantages of fast torque response, small overshoot, and strong robustness against torque loading and parameter variation.

The rest of this article is organized as follows. In Section II, the PMSM mechanical motion equation and electromagnetic equation are given as the basis of the article. The proposed AISMPC and load torque compensation are introduced in Section III. In Section IV, the proposed algorithm is tested on PMSM speed and current regulation system, and the results are compared to the traditional control method FOC, FCS-MPC, SMC, and DB. Finally, Section V summarizes the article.

II. PMSM Mathematical Model

Assuming that the employed PMSM has negligible cross-coupling magnetic saturation, structural asymmetry, iron losses, magnet eddy current loss, and harmonics in the descriptive functions of windings, rotor anisotropy, and coercive force of magnets, the voltage equations of PMSM in the synchronous rotating frame can be described as follows [20]:

$$\begin{cases} \dfrac{di_d}{dt} = \dfrac{1}{L_d}u_d - \dfrac{R}{L_d}i_d + \dfrac{L_q}{L_d}i_q\omega_e \\ \dfrac{di_q}{dt} = \dfrac{1}{L_q}u_q - \dfrac{R}{L_q}i_q - \dfrac{L_d}{L_q}i_d\omega_e - \dfrac{\omega_e\psi_f}{L_q}. \end{cases} \tag{1}$$

In this model, u_d and u_q, respectively, represent the d- and q-axis stator voltages; i_d and i_q, respectively, represent the d- and q-axis currents; L_d and L_q are the stator inductance; R is the winding resistance; ψ_f is the flux linkage of permanent magnets; ω_e is the electrical angular velocity.

The mechanical motion equation and the electromagnetic torque T_e of PMSM are written as follows:

$$\begin{cases} \dfrac{d\omega_m}{dt} = \dfrac{T_e}{J} - \dfrac{T_l}{J} - \dfrac{B\omega_m}{J} \\ T_e = \dfrac{3}{2}P_n[\psi_f i_q + (L_d - L_q)i_d i_q]. \end{cases} \tag{2}$$

In this model, T_e and T_l, respectively, represent the electromagnetic torque and load torque; B represents the viscous damping coefficient; ω_m is the mechanical angular velocity; J is the rotor inertia; P_n is the number of pole pairs. In this article, the surface PMSM is used, L_d is equal to L_q. If the sampling period T of the control system is short enough, the discrete-time model of the PMSM can be described by finite difference approximation series expansion (3). Then, the current in discrete current predictive model of the PMSM is shown in (4)

$$\frac{\mathrm{d}i_{d,q}}{\mathrm{d}t} \approx \frac{i_{d,q}(k+1) - i_{d,q}(k)}{T} \tag{3}$$

$$\begin{cases} i_d(k+1) = \left(1 - \dfrac{RT}{L_d}\right) i_d + \omega_e \dfrac{L_q T}{L_d} i_q + \dfrac{T}{L_d} u_d \\ i_q(k+1) = -\omega_e \dfrac{L_d T}{L_q} i_d + \left(1 - \dfrac{RT}{L_q}\right) i_q \\ \qquad\qquad + \dfrac{T}{L_q} u_q - \omega_e \dfrac{\psi_f}{L_q} T \end{cases} \tag{4}$$

where $i_d(k+1)$ and $i_q(k+1)$ are the state value predicted at the $k+1$ period.

III. Design of Adaptive Integral Sliding-Mode Predictive Control

The proposed system consists of external predictive speed control and inner predictive current control. Fig. 2 illustrates the

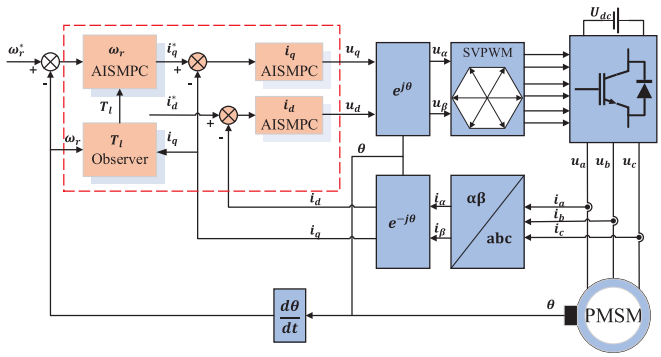

Fig. 2. Overall structure of the proposed AISMPC system.

structure of the system. The details of the design are presented in the following sections.

A. Integral Sliding Surface

Different from the conventional sliding-mode design approaches, the order of the motion equation in integral sliding mode is equal to the order of the original system, rather than reduced by the number of dimensions of the control input. As the result, robustness of the system can be guaranteed throughout an entire response of the system starting from the initial time instance [22], [23]. Especially for multiple differential calculations, the integral structure is necessary. According to the principle of integral sliding mode, the ISMC surface is adopted as follows:

$$s(t) = e(t) + c\int_0^t e(t)dt \tag{5}$$

where $e(t)$ represents the tracking error and $s(t)$ represents the sliding mode surface. c is the integral parameter and $c > 0$.

B. Adaptive Discrete Sliding-Mode Predictive Approach Law

Sliding-mode motion includes approach motion and sliding-mode motion. The motion of the system from any initial state to the switching surface is called the approach motion. According to the sliding-mode variable structure principle, the sliding-mode accessibility condition can only ensure that the moving point from any position in the state space reaches the switching surface in a finite time, and there is no restriction on the specific trajectory of the approaching motion. The approach law method can improve the dynamic quality of the approaching motion.

The exponent reaching law was first proposed and designed by academician Gao *et al.* [11], which can be shown as

$$\frac{ds}{dt} = -\varepsilon \mathrm{sgn}(s) - ks, \varepsilon > 0, k > 0 \tag{6}$$

where $\varepsilon \mathrm{sgn}(s)$ represents the isokinetic reach term; ks represents the index reach term; and ds/dt is the derivative of sliding surface.

According to Taylor series expansion, when the function $f(x)$ is differentiable at the point x_0, there is always

$$f(x) = f(x_0) + f'(x_0)(x - x_0) + o(x - x_0). \tag{7}$$

Because $o(x - x_0)$ is an infinitely small quantity

$$f(x) \approx f(x_0) + f'(x_0)(x - x_0). \tag{8}$$

Similarly to (3), according to forward Euler's discrete formula

$$f(t, x(t)) \approx \frac{x_{t+T} - x_t}{T} \tag{9}$$

$$x(t + T) \approx x(t) + T \cdot f(t, x(t)). \tag{10}$$

According to the design principle of sliding-mode surface, the sliding-mode surface at time $t + T$ can be obtained, which is expressed by the following equation:

$$\begin{cases} s(t + T) = e(t + T) + c\int e(t + T) \\ \dot{s}(t + T) = \dot{e}(t + T) + ce(t + T). \end{cases} \tag{11}$$

The predicted sliding-mode surface after time T can be expressed as

$$\begin{cases} s(t + T) = s(t) + T\dot{s}(t) \\ \dot{s}(t + T) = \dot{s}(t) + T\ddot{s}(t). \end{cases} \tag{12}$$

By combining the model equations (1) and (2) of the system with (11) and (12) of the sliding-mode surface, a sliding-mode predictive controller can be obtained.

It has many advantages to designing the sliding-mode control law of the discrete system by using the discrete approach law. However, under the influence of the parameters of the discrete approach law and the discrete sampling control period, the system will produce a lot of chattering. Therefore, for the sliding-mode predictive control, the discrete adaptive control law is designed to adjust the gain of the control function and reduce chattering.

Then, applying (12) to the time step $t + T$, the chattering analysis of the discrete exponential approximation law for sliding-mode predictive control is presented as follows:

$$\begin{aligned} \dot{s}(t + T) &= \frac{s(t + 2T) - s(t + T)}{T} \\ &= -\varepsilon \mathrm{sgn}[s(t + T)] - k[s(t + T)]. \end{aligned} \tag{13}$$

Solving (13) for $s(t + 2T)$ yields

$$\begin{aligned} s(t + 2T) &= s(t + T) - \varepsilon T \mathrm{sgn}[s(t + T)] - kT[s(t + T)] \\ &= \left(1 - kT - \frac{\varepsilon T}{|s(t + T)|}\right)[s(t + T)]. \end{aligned} \tag{14}$$

From (14), the proportional coefficient p can be obtained to predict the variation trend of sliding-mode surface

$$p = \frac{s(t + 2T)}{s(t + T)} = 1 - kT - \frac{\varepsilon T}{|s(t + T)|} \tag{15}$$

1) $|p| > 1, |s(t + 2T)| > |s(t + T)|$, $s(t)$ is incremental;
2) $|p| = 1, |s(t + 2T)| = |s(t + T)|$, $s(t)$ is self-oscillating;
3) $|p| < 1, |s(t + 2T)| < |s(t + T)|$, $s(t)$ is diminishing.

According to the aforementioned analysis, the sufficient condition for $s(t)$ to decrease is $|p| < 1$. From the aforementioned analysis, we can get the value range of ε as follow:

$$\varepsilon < |s(t + T)| \times (2 - kT) \times \frac{1}{T}. \tag{16}$$

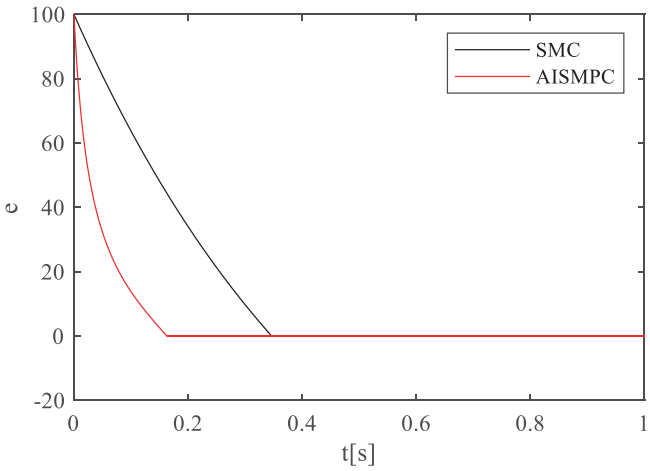

Fig. 3. Convergence rate comparison of SMC and AISMPC.

When the parameter satisfies

$$\begin{cases} \varepsilon = \dfrac{|s(t+T)|}{2} \\ T < \dfrac{4}{1+2k} \end{cases} \tag{17}$$

the inequality (16) is true. Then, the adaptive approach law is

$$\dot{s}(t+T) = -\frac{|s(t+T)|}{2}\mathrm{sgn}[s(t+T)] - k[s(t+T)]. \tag{18}$$

Therefore, according to the amplitude of the sliding mode surface, the controller can adjust the output command signal to achieve a faster dynamic response and smaller steady-state chattering. By invoking the normal Euler forward method, the discrete convergence process of SMC and AISMPC can be simplified described as follows.

1: Initialization:
2: $T = 62.5e-6\mu s, f = 16kHz$
3: $e = 0, \tilde{e} = 0$
4: Measurement: ω_r, i_d, i_q
5: for $j = 1 : n$
6: Sliding mode surface calculation:
7: $s(j) = e(j)$
8: $\tilde{s}(j) = \tilde{e}(j)$
9: Reaching law calculation:
10: $s(j+1) = s(j) + (-\varepsilon\,\mathrm{sgn}(s(j)) - ks(j))T$
11: $\tilde{s}(j+1) = \tilde{s}(j) + (-\varepsilon\,\mathrm{sgn}(\tilde{s}(j)) - k\tilde{s}(j))T$
12: $\tilde{s}(j+2) = \tilde{s}(j+1)$
13: $+\left(-\frac{|\tilde{s}(j+1)|}{2}\,\mathrm{sgn}(\tilde{s}(j+1)) - k\tilde{s}(j+1)\right)T$
14: end

Fig. 3 shows the performance of convergence and equilibrium point of SMC and AISMPC. It can be seen that AISMPC achieves faster convergence rate.

The stability of the algorithm is proved as follows:

$$V(k) = \frac{1}{2}s^2(t). \tag{19}$$

As long as the conditions are met

$$\Delta V(t) = s^2(t+T) - s^2(t) < 0, s(k) \neq 0. \tag{20}$$

$s(t) = 0$ is globally asymptotically stable equilibrium surface, that is, any initial position state tends to switch surface $s(t)$. The following conditions need to be met:

$$s^2(t+T) < s^2(t). \tag{21}$$

When the sampling time T is small enough, the existence and arrival conditions of the discrete sliding mode are as follows:

$$\begin{aligned} &[s(t+T) - s(t)]\,\mathrm{sgn}(s(t)) < 0 \\ &[s(t+T) + s(t)]\,\mathrm{sgn}(s(t)) > 0 \end{aligned} \tag{22}$$

$$\begin{aligned} &[s(t+T) - s(t)]\,\mathrm{sgn}(s(t)) \\ &= \left(-kTs(t) - \frac{|s(t)|}{2}\,\mathrm{Tsgn}(s(t))\right)\mathrm{sgn}(s(t)) \\ &= -(k+0.5)T|s(t)| < 0 \end{aligned} \tag{23}$$

$$\begin{aligned} &[s(t+T) + s(t)]\,\mathrm{sgn}(s(t)) \\ &= \left((2-kT)s(t) - \frac{|s(t)|}{2}\,\mathrm{Tsgn}(s(t))\right)\mathrm{sgn}(s(t)) \\ &= (2 - 0.5T - kT)|s(t)| > 0. \end{aligned} \tag{24}$$

The method of sliding mode meets the existence and arrival condition of the discrete sliding mode, and the designed control system is stable.

C. Design of Load Disturbance Compensation

PMSM dynamic space-state equation

$$\begin{cases} \dot{x} = Ax + Bu + Df \\ y = Cx \end{cases} \tag{25}$$

where x is state vector; u is control input; f is disturbance; A, B, and D are matrix of the coefficients.

The disturbance can be expressed as

$$Df = \dot{x} - Ax - Bu. \tag{26}$$

If the rate of change of disturbance f is 0, the estimate of disturbance is the general design principle of the disturbance observer. The error e_f of the disturbance between real value f and the estimated value $\hat{f}$ is defined as

$$e_f = \hat{f} - f. \tag{27}$$

When the observed value is very close to the actual value, the disturbance observer can be constructed as follows:

$$\dot{\hat{f}} = -k_f(D\hat{f} - Df) = -k_f[D\hat{f} - (\dot{x} - Ax - Bu)] \tag{28}$$

where k_f is observer gain coefficient.

In order to facilitate computation, the intermediate variable matrix M can be expressed as

$$M = \hat{f} - k_f x \tag{29}$$

$$\begin{aligned} \dot{M} &= \dot{\hat{f}} - k_f\dot{x} = -k_f[D\hat{f} - (\dot{x} - Ax - Bu)] - k_f\dot{x} \\ &= -k_f(D\hat{f} - Ax - Bu). \end{aligned} \tag{30}$$

And then, the structure of the disturbance observer is described in

$$\hat{f} = k_f x + \int \dot{M} = k_f x + \int -k_f(D\hat{f} - Ax - Bu). \quad (31)$$

According to the PMSM motion equation (2) and aforementioned design principle of the observer, the calculated value of load torque of PMSM is

$$\hat{T_l} = k_f \omega_m - \int k_f \left(-\frac{1}{J}\hat{T_l} + \frac{B}{J}\omega_m - \frac{3P_n\psi_f}{2J} i_q \right). \quad (32)$$

The load torque observer needs to meet Lyapunov stability conditions, which are proved as follows. According to (27) and (28), the torque observation error equation of PMSM can be obtained as follows:

$$\dot{e}_T - k_f e_T/J = 0 \quad (33)$$

$$e_T = \hat{T_l} - T_l. \quad (34)$$

The constraint equation of stability is

$$\dot{V} = e_T \dot{e}_T = k_f e_T^2/J < 0. \quad (35)$$

Then, the stability condition of the load torque observer is $k_f < 0$.

D. Design of the AISMPC Speed and Current Controller

To sum up, the following speed controller is designed by combining the AISMPC and torque observation compensation. First, the sliding-mode surface of the speed controller is obtained according to the mechanical motion equation and torque equation of the motor

$$\begin{cases} s_\omega = c_\omega \int e_\omega + e_\omega = c_\omega \int (\omega_m^* - \omega_m) + (\omega_m^* - \omega_m) \\ \dot{s}_\omega = c_\omega e_\omega + \dot{e}_\omega = c_\omega (\omega_m^* - \omega_m) - \dot{\omega}_m \\ \ddot{s}_\omega = c_\omega \dot{e}_\omega + \ddot{e}_\omega = c_\omega (-\dot{\omega}_m) - \left(\dfrac{3P_n\psi_f}{2J} \dot{i}_q - \dfrac{B\dot{\omega}_m}{J} \right). \end{cases} \quad (36)$$

According to (12) and (36), following equation can be obtained:

$$\begin{aligned} &\dot{s}(t+T) = \dot{s}(t) + T\ddot{s}(t) \\ &= \dot{s}_\omega(t) + T\left(\frac{B}{J} - c_\omega\right)\dot{\omega}_m - T\left(\frac{3P_n\psi_f}{2J}\right)\dot{i}_q(t). \end{aligned} \quad (37)$$

The approach law equation (18) is equal to the sliding mode surface equation (37), and the following equation can be obtained:

$$\begin{aligned} &\dot{s}_\omega(t) + T\left(\frac{B}{J} - c_\omega\right)\dot{\omega}_m(t) - T\left(\frac{3P_n\psi_f}{2J}\right)\dot{i}_q(t) \\ &= -\frac{|s_\omega(t+T)|}{2}\operatorname{sgn}[s_\omega(t+T)] - k[s_\omega(t+T)]. \end{aligned} \quad (38)$$

According to (2), the load torque on the motor can be regarded as external disturbance. The accurate estimation of load torque is conducive to improving the response performance of the motor in the dynamic loading process. In particular, when the load changes, the torque feed-forward structure can compensate the action of the controller, thereby reducing the response time.

The change of load torque will cause the change of i_q, so the disturbance compensation value can be calculated to compensate the current i_q. The observed torque can be obtained from (32). The current compensation value i_{qd}, and the output value of AISMPC $i_q^\sim$ can be calculated as follows:

$$i_{qd} = \frac{2\hat{T_l}}{3P_n\psi_f} \quad (39)$$

$$i_q^* = i_q^\sim + i_{qd}. \quad (40)$$

Similarly, according to the current equation (1) in the $d-q$ coordinate system, the sliding-mode surface of the controller mathematical equations can be expressed

$$\begin{cases} s_q = c_q \int e_q = c_q \int (i_q^* - i_q) \\ \dot{s}_q = c_q e_q = c_q (i_q^* - i_q) \\ \ddot{s}_q = c_q \dot{e}_q = c_q (-\dot{i}_q) \end{cases} \quad (41)$$

$$\begin{cases} s_d = c_d \int e_d = c_d \int (i_d^* - i_d) \\ \dot{s}_d = c_d e_d = c_d (i_d^* - i_d) \\ \ddot{s}_d = c_d \dot{e}_d = c_d (-\dot{i}_d). \end{cases} \quad (42)$$

The following equation can be obtained by combining the mathematical model of the motor and the principle of sliding-mode predictive control:

$$\begin{aligned} &\dot{s}_q(t) - Tc_q\frac{1}{L_q}[u_q(t) - Ri_q(t) - L_d i_d(t)\omega_e(t) - \omega_e(t)\psi_f] \\ &= -\frac{|s_q(t+T)|}{2}\operatorname{sgn}[s_q(t+T)] - k[s_q(t+T)] \end{aligned} \quad (43)$$

$$\begin{aligned} &\dot{s}_d(t) - Tc_d\frac{1}{L_d}[u_d(t) - Ri_d(t) + L_q i_q(t)\omega_e(t)] \\ &= -\frac{|s_d(t+T)|}{2}\operatorname{sgn}[s_d(t+T)] - k_d[s_d(t+T)]. \end{aligned} \quad (44)$$

The voltage equation in the $d-q$ coordinates system can be expressed as

$$\begin{aligned} u_q(t) = &\left\{ -\frac{|s_q(t+T)|}{2}\operatorname{sgn}[s_q(t+T)] - k_q[s_q(t+T)] \right. \\ &\left. - \dot{s}_q(t) \right\} \Big/ \left(-\frac{Tc_q}{L_q} \right) + [Ri_q(t) + L_d i_d(t)\omega_e(t) + \omega_e(t)\psi_f] \end{aligned} \quad (45)$$

$$\begin{aligned} u_d(t) = &\left\{ -\frac{|s_d(t+T)|}{2}\operatorname{sgn}[s_d(t+T)] - k_d[s_d(t+T)] \right. \\ &\left. - \dot{s}_d(t) \right\} \Big/ \left(-\frac{Tc_d}{L_d} \right) + [Ri_d(t) - L_q i_q(t)\omega_e(t)]. \end{aligned} \quad (46)$$

According to (38), (45), and (46), the AISMPC algorithm of speed loop and current loop is constructed, respectively. To further improve the response speed, the disturbance compensation

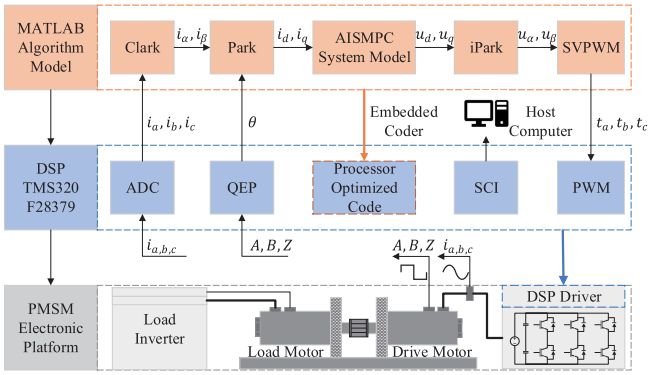

Fig. 4. Block diagram of the designed DSP-based experimental platform.

TABLE I
PARAMETERS OF PMSM

Descriptions	Symbol	Values	Unit
Rated Power	P_n	3.8	kW
Rated Speed	ω_{rN}	1500	rpm
Rated Torque	T_{MN}	24	Nm
Nominal Voltage	V_N	362	V
Rated Current	I_N	7.4	A
Stator Resistance	R	1.32	Ω
Stator Inductance	L_d	13.6	mH
Stator Inductance	L_q	13.6	mH
Pole Pairs	P_n	4	
PM Flux	ψ_f	0.45	Wb
Rotor Inertia	J	0.002	$kg \cdot m^2$
Friction Coefficient	B	0.008	$N \cdot m \cdot s$
DC Link Voltage	V_{dc}	512	V

algorithm is constructed. Finally, the AISMPC is realized by the output control signal of the space vector pulse width modulation (SVPWM) section.

IV. EXPERIMENTAL VERIFICATION

In this section, to demonstrate the effectiveness of AISMPC, the experimental contrast of FOC, PTC, SMC, DB, and the AISMPC in the same PMSM system was carried out. Steady-state loading tests and dynamic loading tests are carried out, respectively. The validity of the proposed method can be verified by the total harmonic distortion of the current and the dynamic response time of the rotation speed.

A. System Structure and Test Bench

To verify the practicability and validity of AISMPC, the experiment is carried out on a 3.8-kW PMSM test bench. The parameters of the PMSM are given in Table I. In the experimental test bench, a TMS320F28379D digital signal processor (DSP) is employed for algorithm implementation. The control frequency of the system is 16 kHz and the sampling time is 62.5 μs. Fig. 4 shows the block diagram of the designed DSP-based experimental platform. Fig. 5 shows the hardware platform of the system.

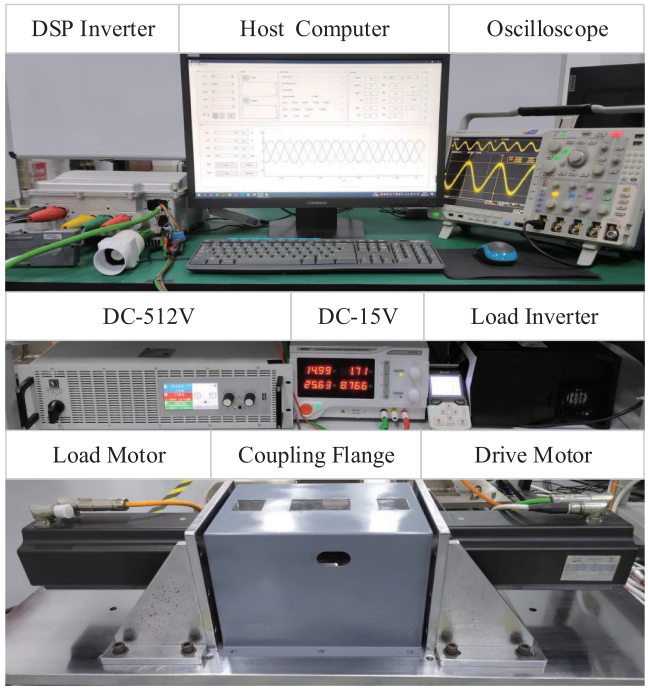

Fig. 5. PMSM test bench.

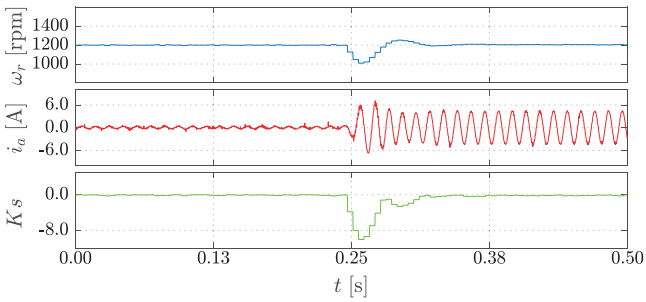

Fig. 6. Experimental results: The parameter Ks adjustment process at 1200 r/min, 12-N·m torque loading.

B. Parameter Adaptive Adjustment Process

AISMPC is an organic combination of sliding-mode predictive control and adaptive control. In this section, the changes in rotation speed, current, and parameters during the dynamic loading process will be shown. Fig. 6 shows the parameter adjustment process during the torque-loading process. At the speed of 1200 r/min, a load torque of 12 N·m is suddenly added. For the figure set, variables from the top down to the bottom are speed ω_r, current of phase-a i_a, and adaptive parameter Ks. Ks is the amplitude variation of a sign function in the control law. It can be seen from the figure that in the process of loading, the speed tracking error increases, and the sliding-mode surface amplitude increases. To achieve a better adjustment effect, the coefficient Ks adjusts the amplitude along with the sliding-mode surface to improve the dynamic response of the system.

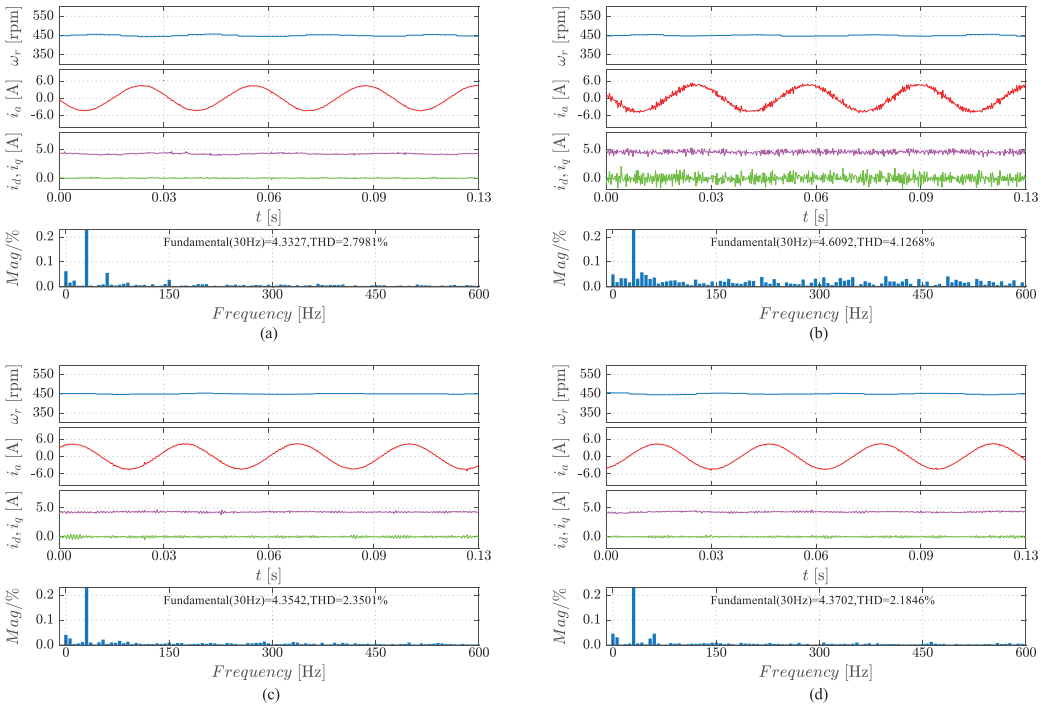

Fig. 7. Experimental results: Process of steady state of current control at 450 r/min and 12 N·m. (a) PI-PI. (b) PI-PTC. (c) PI-ISMPC. (d) PI-AISMPC.

C. Steady-State Performance Comparison

To verify the effectiveness of the proposed scheme, the experiments of the speed loop controller and the current loop controller are carried out, respectively. In the comparison of the steady-state current loop, the external loop is set as a unified PI control, and different controllers are used in the current loop. In the comparison of steady-state speed loops, the inner loop is set as a unified PI control. Finally, the controllers of different control loops can be analyzed separately.

1) Comparison of Current Controllers: The steady-state control precision of the system is an important factor in motor control. In this section, to verify the steady-state performance of the proposed AISMPC algorithm, PI is adopted for the speed control loop. At the same time, PI, PTC, ISMPC, and the proposed method are used in the current loop, respectively. The THD of each control condition is analyzed to compare the steady-state accuracy of the controller.

In the steady-state process, Fig. 7 demonstrates a comparison of the current control, where the speed is 450 r/min and the load torque is 12 N·m. For each figure set, variables from the top down to the bottom are speed ω_r, current of phase-a i_a, d- and q-axis current i_d, i_q and total harmonic distortion. The control strategy for comparison is (a) PI-PI, (b) PI-PTC, (c) PI-ISMPC, and (d) PI-AISMPC. To show the difference between the algorithms, the same set of PI parameters were used for the speed loop. The results show that AISMPC can effectively improve the control accuracy of the current with the smallest THD value of 2.1846%.

2) Comparison of Speed Controllers: To make a speed loop controller's comparison, the current loop is regulated by the PI controller. The proposed strategy, respectively, compared with SMC, ISMPC, and analyzes its steady-state performance.

In the steady-state experiment, Fig. 8 presents the precision comparison of the speed control, where the speed is 450 r/min and the load torque is 12 N·m. For each figure set, variables from the top down to the bottom are speed ω_r, current of phase-a i_a, d- and q-axis current i_d, i_q and total harmonic distortion. The control strategy for comparison is (a) SMC-PI, (b) ISMPC-PI, (c) AISMPC-PI, and (d) AISMPC-AISMPC. According to the aforementioned experimental data, the steady-state characteristics of the rotating speed loop are improved after adopting the proposed scheme. The ISMPC showed a significant improvement over SMC, with THD reduced from 2.832% to 2.277%.

3) Comparison of THD: Combined with the previous experimental data, the steady-state summary results are obtained. According to Fig. 9, since there is no SVPWM for the model predictive torque control, this control method has higher harmonic content. In this experiment, the harmonic content is 4.1268% and the steady-state accuracy of the system is greatly affected. PI control is a relatively classic control, but under different conditions, different PI parameter settings will also have a large difference in control results. In this experiment, a set of speed loop PI parameters with good performance is adopted, among which K_p is 0.02 and K_i is 3. In sliding-mode control, the excessive gain of sign function can improve the response speed, but at the same time bring chattering to the system. The SMC experiment's THD is 2.8326%. To solve the problems of the aforementioned controllers and balance the dynamic and steady performance, the AISMPC strategy is proposed. ISMPC can effectively reduce the harmonic content of the system. In order to further reduce the chattering of the system, AISMPC can reduce THD to 1.917%, which greatly promoted the control accuracy. Due to the effect of adaptive parameter regulation, the amplitude of sign function is small in steady state, and there is

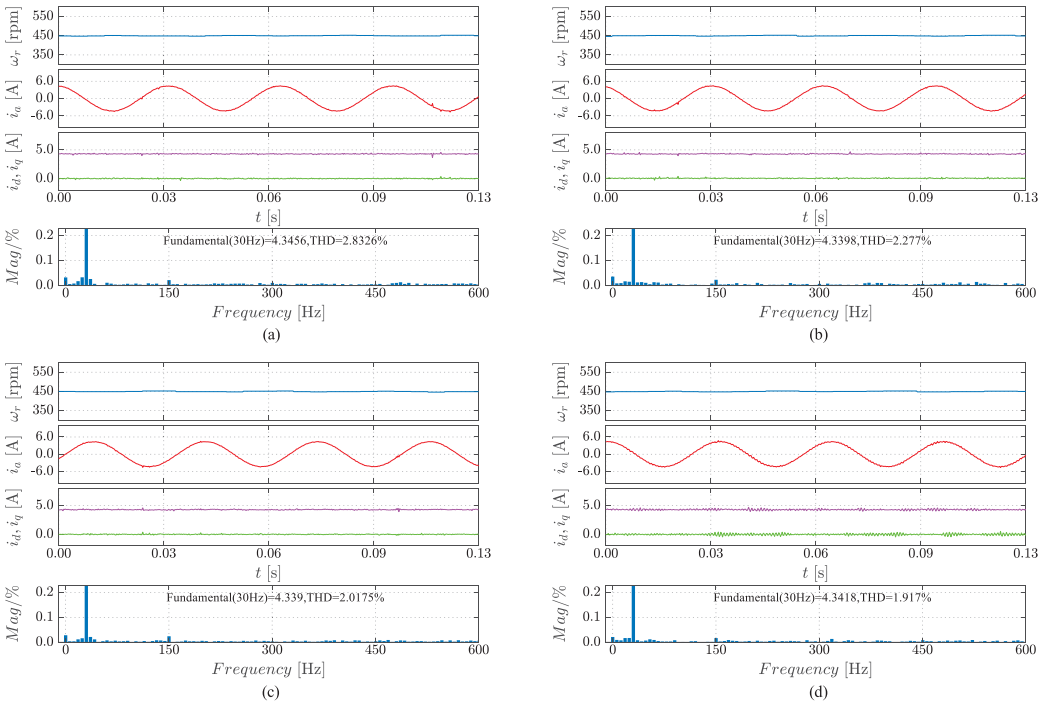

Fig. 8. Experimental results: Process of steady state of speed control at 450 r/min and 12 N·m. (a) SMC-PI. (b) ISMPC-PI. (c) AISMPC-PI. (d) AISMPC-AISMPC.

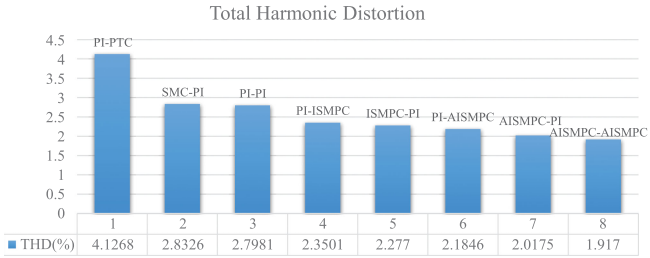

Fig. 9. Total harmonic distortion comparison.

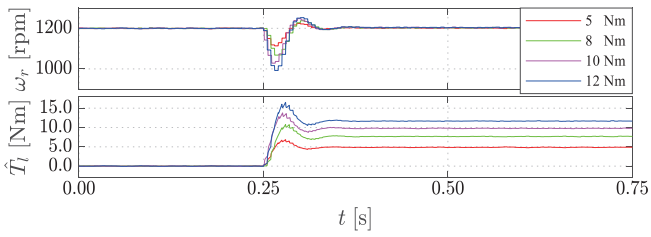

Fig. 10. Experimental results: The control algorithm adopted is AISMPC-AISMPC. Torque loading process from 0 to 5, 8, 10, and 12 N·m.

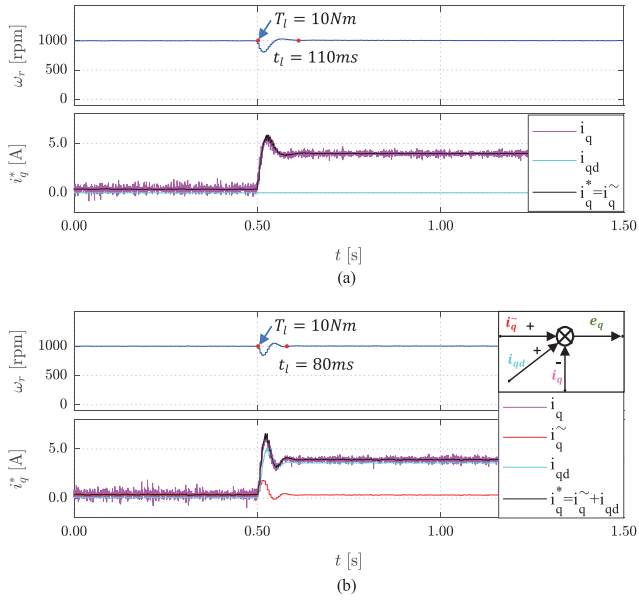

Fig. 11. Experimental results: Torque feed-forward compensation. (a) The state of AISMPC control. (b) The state of AISMPC control with torque feed-forward compensation.

no chattering phenomenon caused by sliding-mode structure. Therefore, the AISMPC algorithm can greatly improve the steady-state performance of the system.

D. Dynamic State Performance

1) Torque Observation Process: Fig. 10 demonstrates the torque variation and observation process. It can be seen from Fig. 10 that when the rotation speed is 1200 r/min and the initial torque is 0 N·m, the load is suddenly increased to 5, 8, 10, 12 N·m. Under different loads, AISMPC controller can realize fast tracking of target speed. The torque observer can realize the tracking of the torque change in the dynamic response process.

2) Torque feed-forward compensation: The ability of the system to resist disturbance is important. This article combines a feed-forward compensation method as shown in Fig. 11(b). At the moment of torque loading, the signal i_{qd} is calculated to compensate the speed controller's output signal $i_q^{\sim}$. According

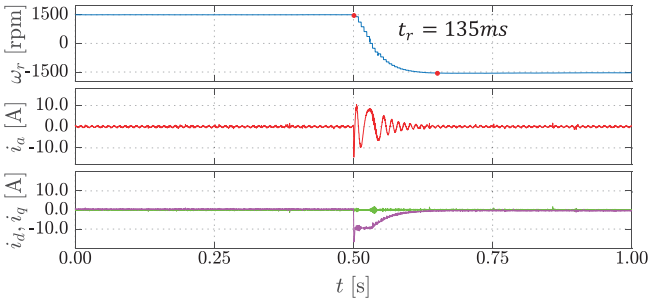

Fig. 12. Experimental results: The control algorithm adopted is AISMPC-AISMPC. Speed reversion process from 1500 to -1500 r/min.

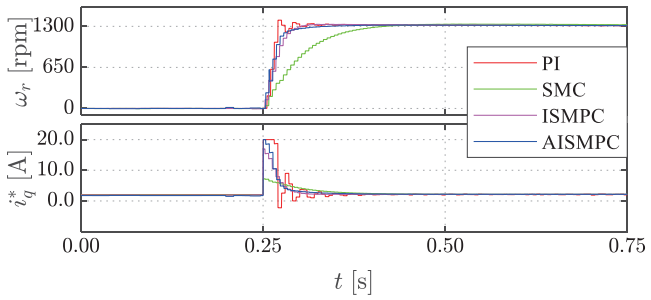

Fig. 13. Experimental results: Speed startup response process from 0 to 1300 with loading torque 5 N·m.

to (40), the feed-forward structure is established. As shown in Fig. 11(a), the AISMPC torque loading response time is 110 ms. To further reduce the response time of the system, torque feed-forward compensation structure is designed. When the system is compensated, the response time reduced to 80 ms. The experimental results show that the proposed method improves the antidisturbance ability of the system.

3) Speed Reversion Experiment: Fig. 12 demonstrates the speed reversion performance from 1500 to -1500 r/min without load. The speed reference revers at 0.5 s and the torque changes quickly to meet the needs of fast speed reversion. It takes 135 ms to complete speed reversion without overshoot. In the experiment of rotational speed reversal, the proposed strategy still responds quickly. From the previous experiments, it can be concluded that AISMPC can realize fast response of rotational speed without overshoot, satisfying the required control effect.

4) Speed Startup Response Experiment: To verify the speed startup response of the proposed method, the comparison experiments of different speed loop algorithms are carried out. Fig. 13 shows the speed ω_r and q-axis current i_q responses at the reference speed of 1300 r/min and the torque loading of 5 N·m. The speed loop controller is PI, SMC, ISMPC, and AISMPC, separately. To ensure the validity of the comparison, AISMPC algorithm is used for the current loop. As shown in Fig. 13, PI control has a faster response speed, but there is a large overshoot. The response speed of SMC is slow and the time to reach the target speed is 166 ms. ISMPC and AISMPC have the same sliding-mode predictive structure, only the adaptive parameter K_s is different. Because of the adjustment of the adaptive parameters, the current is larger at the moment of acceleration. When a given speed is reached, the control's output is smaller and the current is more stable. AISMPC method achieves a balance between velocity and smoothness.

5) Load Disturbance Performance: In the process of system torque loading, the external response speed of the control system is very important. To verify the antidisturbance performance of the system, the experimental comparison of torque loading is carried out. In this experiment, the torque feed-forward compensation method is adopted, and the control effects of different controllers are compared. Fig. 14 shows that the comparison of dynamic loading processes of different control strategies. The rotation speed is 1500 r/min, and the load torque increased from 0 to 12 N·m suddenly. For each figure set, variables from the top down to the bottom are speed ω_r, current of phase-a i_a, d- and q-axis current i_d, i_q. The control strategy for comparison is (a) SMC-PI, (b) PI-DB, (c) ISMPC-ISMPC, and (d) AISMPC-AISMPC.

By comparing the aforementioned experimental data, AISMPCs response is faster in the process of torque loading. Compared with the sliding-mode control, there is no steady-state error. Compared with DB, regulating time is shorter. Compared with the integral sliding-mode predictive control, the proposed scheme reaches a steady-state within a short period of time. The load response time of AISMPC is 69 ms and the load reduction response time is only 80 ms. Compared with other control strategies, the effect is significant. To sum up, AISMPC can achieve a better dynamic response. The experimental results validate the previous design and hypothesis.

E. PMSM Parameter Mismatch Experiment

Nonlinear factors and temperature changes in the PMSM control system will lead to model parameter mismatch, which will weaken the robustness and dynamic response of speed and current predictive control. In this section, motor model parameter mismatch in PMSM sliding-mode predictive control is analyzed. The influence of resistance, inductance, flux linkage, inertia, friction coefficient on the stability of the mismatched system was investigated. The results show that the adaptive integral sliding-mode predictive control still has good robustness in the case of parameter mismatch, which provides strong support for the accuracy of predictive control of PMSM.

Fig. 15 illustrates the parameter mismatch experiment results of AISMPC method, where the speed is 1000 r/min and the load torque is 12 N·m. For each figure set, variables from the top down to the bottom are speed ω_r, current of phase-a i_a, the ratio of parameter mismatches. The dynamic characteristics of 6 groups of parameters (R, L_d, L_q, ψ_f, J, B) were compared under the condition of parameter mutation. In the initial stage, the parameter is less than the standard parameter. In the intermediate stage, it is the standard parameter, and in the final stage, it is greater than the standard parameter. The black lines in the figure represent the ratio of set parameters to standard parameters. It can be seen from the experimental results that the system still has good robustness under the condition of parameter mismatch. At the instant of the parameter mutation, the mismatch parameters can affect the calculation of torque and the output value of

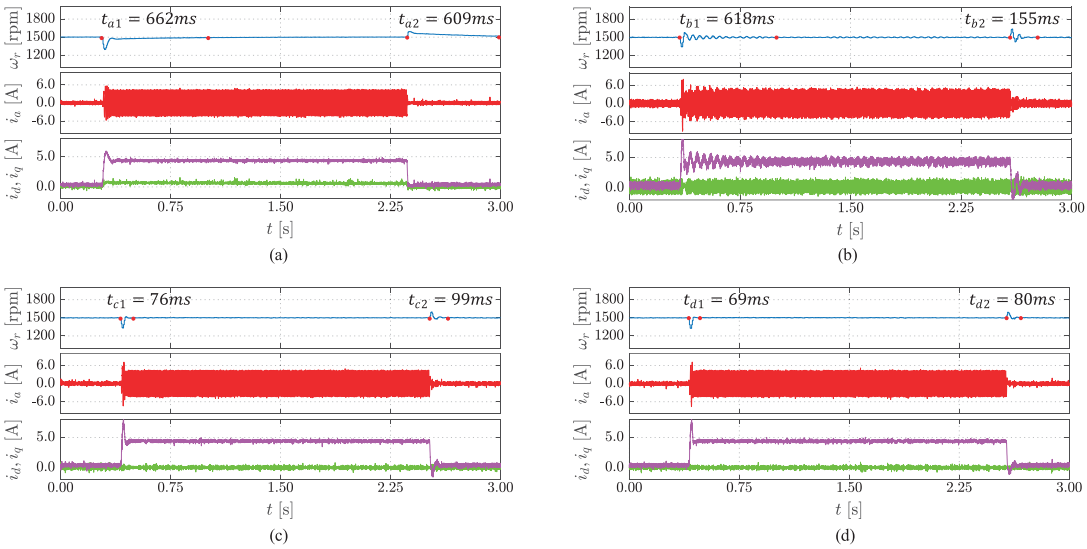

Fig. 14. Experimental results: Process of dynamic loading at 1500 r/min and 12 N·m. (a) SMC-PI. (b) PI-DB. (c) ISMPC-ISMPC. (d) AISMPC-AISMPC.

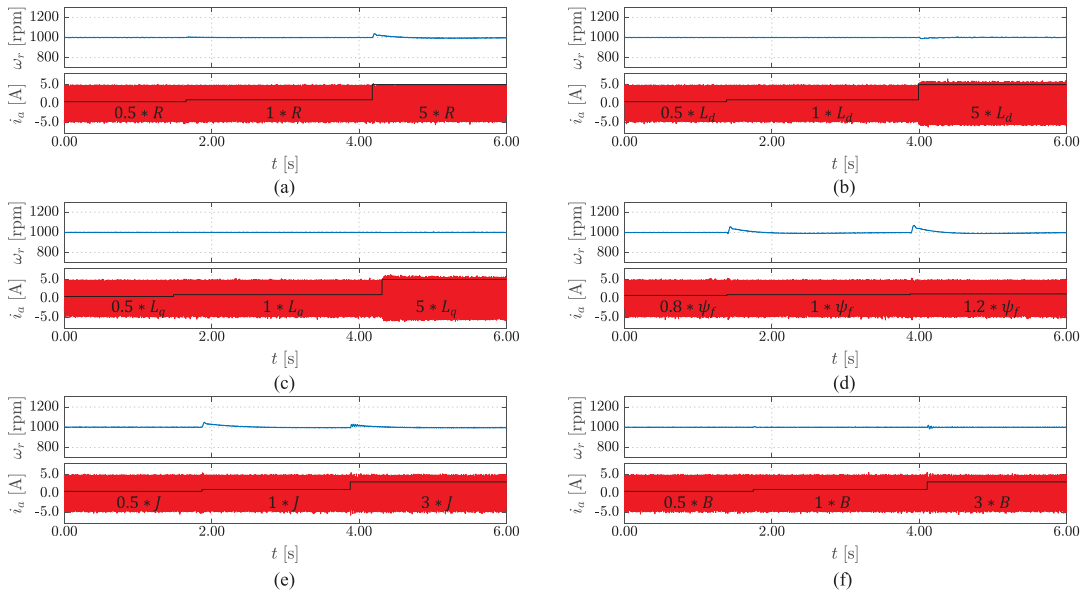

Fig. 15. Experimental results: Motor parameter mismatch experiment at 1000 r/min and 12 N·m. (a) R. (b) L_d. (c) L_q. (d) ψ_f. (e) J. (f) B.

algorithm. But because the system has robust characteristics of sliding-mode structure, the system can still track the target of the control signal and satisfy the requirement of the system robustness.

V. Conclusion

This article presents a robust continuous model predictive speed and current control for PMSM with an adaptive integral sliding-mode approach. Compared with traditional MPC, the proposed control method has no weighting coefficient. In addition, AISMPC has better performance in both inner current loop and external speed loop. Especially, it has characteristics of fast response of predictive control and robustness of sliding-mode control. Adaptive control reduces the chattering of sliding-mode control and disturbance compensation improves the antidisturbance ability of the system. Experimental results confirm that the proposed system has better performance in a wide speed range and faster response with load torque disturbance. By considering the improvement of eliminating chattering, a high-order SMPC will be verified in future work.

References

[1] D. Casadei, F. Profumo, G. Serra, and A. Tani, "FOC and DTC: Two viable schemes for induction motors torque control," *IEEE Trans. Power Electron.*, vol. 17, no. 5, pp. 779–787, Sep. 2002.

[2] P. Karamanakos and T. Geyer, "Guidelines for the design of finite control set model predictive controllers," *IEEE Trans. Power Electron.*, vol. 35, no. 7, pp. 7434–7450, Jul. 2020.

[3] F. Wang, S. Li, X. Mei, W. Xie, J. Rodríguez, and R. M. Kennel, "Model-based predictive direct control strategies for electrical drives: An experimental evaluation of PTC and PCC methods," *IEEE Trans. Ind. Informat.*, vol. 11, no. 3, pp. 671–681, Jun. 2015.
[4] F. Wang, K. Zuo, P. Tao, and J. Rodriguez, "High performance model predictive control for PMSM by using stator current mathematical model self-regulation technique," *IEEE Trans. Power Electron.*, vol. 35, no. 12, pp. 13652–13662, Dec. 2020.
[5] B. Guo, S. Bacha, and M. Alamir, "A review on ADRC based PMSM control designs," in *Proc. IECON 43rd Annu. Conf. Ind. Electron. Soc.*, 2017, pp. 1747–1753.
[6] S. Kim, K. Lee, and K. Lee, "Singularity-free adaptive speed tracking control for uncertain permanent magnet synchronous motor," *IEEE Trans. Power Electron.*, vol. 31, no. 2, pp. 1692–1701, Feb. 2016.
[7] X. Cai, Z. Zhang, J. Wang, and R. Kennel, "Optimal control solutions for PMSM drives: A comparison study with experimental assessments," *IEEE Trans. Emerg. Sel. Top. Power Electron.*, vol. 6, no. 1, pp. 352–362, Mar. 2018.
[8] S. Li and H. Gu, "Fuzzy adaptive internal model control schemes for PMSM speed-regulation system," *IEEE Trans. Ind. Informat.*, vol. 8, no. 4, pp. 767–779, Nov. 2012.
[9] F. Mendoza-Mondragón, V. M. Hernández-Guzmán, and J. Rodríguez-Reséннdiz, "Robust speed control of permanent magnet synchronous motors using two-degrees-of-freedom control," *IEEE Trans. Ind. Electron.*, vol. 65, no. 8, pp. 6099–6108, Aug. 2018.
[10] V. Utkin, "Variable structure systems with sliding modes," *IEEE Trans. Autom. Control*, vol. AC-22, no. 2, pp. 212–222, Apr. 1977.
[11] W. Gao, Y. Wang, and A. Homaifa, "Discrete-time variable structure control systems," *IEEE Trans. Ind. Electron.*, vol. 42, no. 2, pp. 117–122, Apr. 1995.
[12] A. Bartoszewicz and K. Adamiak, "Discrete-time sliding-mode control with a desired switching variable generator," *IEEE Trans. Autom. Control*, vol. 65, no. 4, pp. 1807–1814, Apr. 2020.
[13] Y. Wang, Y. Feng, X. Zhang, and J. Liang, "A new reaching law for antidisturbance sliding-mode control of PMSM speed regulation system," *IEEE Trans. Power Electron.*, vol. 35, no. 4, pp. 4117–4126, Apr. 2020.
[14] A. K. Junejo, W. Xu, C. Mu, M. M. Ismail, and Y. Liu, "Adaptive speed control of PMSM drive system based a new sliding-mode reaching law," *IEEE Trans. Power Electron.*, vol. 35, no. 11, pp. 12 110–12121, Nov. 2020.
[15] Y. Eldigair, A. R. Beig, and J. Alsawalhi, "Sensorless DTSMC of a three-level VSI fed PMSM drive," *IET Power Electron.*, vol. 13, no. 4, pp. 788–797, 2020.
[16] J. Yang, J. Su, S. Li, and X. Yu, "High-order mismatched disturbance compensation for motion control systems via a continuous dynamic sliding-mode approach," *IEEE Trans. Ind. Informat.*, vol. 10, no. 1, pp. 604–614, Feb. 2014.
[17] I. M. Hassine, M. W. Naouar, and N. Mrabet-Bellaaj, "Model predictive-sliding mode control for three-phase grid-connected converters," *IEEE Trans. Ind. Electron.*, vol. 64, no. 2, pp. 1341–1349, Feb. 2017.
[18] J. Wang, F. Wang, Z. Zhang, S. Li, and J. Rodríguez, "Design and implementation of disturbance compensation-based enhanced robust finite control set predictive torque control for induction motor systems," *IEEE Trans. Ind. Informat.*, vol. 13, no. 5, pp. 2645–2656, Oct. 2017.
[19] L. He, F. Wang, J. Wang, and J. Rodríguez, "ZYNQ implemented Luenberger disturbance observer based predictive control scheme for PMSM drives," *IEEE Trans. Power Electron.*, vol. 35, no. 2, pp. 1770–1778, Feb. 2020.
[20] X. Zhang, B. Hou, and Y. Mei, "Deadbeat predictive current control of permanent-magnet synchronous motors with stator current and disturbance observer," *IEEE Trans. Power Electron.*, vol. 32, no. 5, pp. 3818–3834, May 2017.
[21] B. Wang, C. Luo, Y. Yu, G. Wang, and D. Xu, "Antidisturbance speed control for induction machine drives using high-order fast terminal sliding-mode load torque observer," *IEEE Trans. Power Electron.*, vol. 33, no. 9, pp. 7927–7937, Sep. 2018.
[22] Y. Pan, C. Yang, L. Pan, and H. Yu, "Integral sliding mode control: Performance, modification, and improvement," *IEEE Trans. Ind. Informat.*, vol. 14, no. 7, pp. 3087–3096, Jul. 2018.
[23] V. Utkin and J. Shi, "Integral sliding mode in systems operating under uncertainty conditions," in *Proc. 35th IEEE Conf. Decis. Control*, vol. 4, 1996, pp. 4591–4596.

Zheng Li was born in Tai'an, China, in 1991. He received the B.S. degree in electronic information engineering and the M.S. degree in control engineering from the North University of China, Taiyuan, China, in 2015 and 2018, respectively. He is currently working toward the Ph.D. degree with the Quanzhou Institute of Equipment Manufacturing, Haixi Institutes, Chinese Academy of Sciences, Beijing, China.

His research interests include predictive control and optimal control for electrical drives.

Fengxiang Wang (Senior Member, IEEE) was born in Jiujiang, China, in 1982. He received the B.S. degree in electronic engineering and the M.S. degree in automation from Nanchang Hangkong University, Nanchang, China, in 2005 and 2008, respectively, and the Ph.D. degree from the Institute for Electrical Drive Systems and Power Electronics, Technische Universität München, Munich, Germany, in 2014.

He is currently a Full Professor and the Deputy Director of the Quanzhou Institute of Equipment Manufacturing, Haixi Institutes, Chinese Academy of Sciences, Jinjiang, China. His research interests include predictive control and sensorless control for electrical drives and power electronics.

Dr. Wang is an IET Fellow, and an Associate Editor for the IEEE TRANSACTIONS ON INDUSTRIAL ELECTRONICS and IEEE TRANSACTIONS ON ENERGY CONVERSION. As the General Chair, he organized IEEE 5th International Symposium on Predictive Control of Electrical Drives and Power Electronics (PRECEDE).

Dongliang Ke was born in Quanzhou, China, in 1986. He received the B.S. degree in electrical engineering and the M.S. degree in power electronics and power drives from Northwestern Polytechnical University, Xi'an, China, in 2010 and 2013, respectively.

He is currently working with Haixi Institutes, Chinese Academy of Sciences, China. His research interests include predictive control for electrical drives.

Jiaxiang Li was born in Zhumadian, China, in 1996. He received the B.S. degree from the Jiangsu University of Science and Technology, Zhenjiang, China, in 2018. He is currently working toward the M.S. degree with the College of Electrical Engineering and Automation, Fuzhou University, Fuzhou, China.

His research interests include model predictive control for electrical drive system and intelligent optimization algorithm.

Wei Zhang was born in Anhui, China, in 1983. He received the B.S. degree in informatik from Universität Stuttgart, Stuttgart, Germany, in 2008, and the M.S. degree in automotive software engineering from Technische Universität Chemnitz, Chemnitz, Germany, in 2012. He is currently working toward the Ph.D. degree with the Institute for Electrical Drive Systems and Power Electronics, Technische Universität München, Munich, Germany.

He is currently the Director of Intelligent Manufacturing Department and Energy Management Department, Contemporary Amperex Technology Company, Ltd., China. He is also a Guest Professor with the Institute for Mechanical Engineering and Automation, Fuzhou University, Fuzhou, China. His research interests include learning-based control theory for electrical drives, robotics, mechanical system, laser system, and deep learning in industrial computer vision.